IEEE Access
Multidisciplinary | Rapid Review | Open Access Journal

Received October 20, 2021, accepted November 2, 2021, date of publication November 8, 2021, date of current version November 15, 2021.

Digital Object Identifier 10.1109/ACCESS.2021.3125688

Dual Stator Permanent Magnet Vernier Machine With Yokeless Rotor Having Single Stator Winding for Torque Density Improvement

MUDASSIR RAZA SIDDIQI[1], TANVEER YAZDAN[2], JUN-HYUK IM[1], (Student Member, IEEE), YEOL-KYEONG LEE[1], AND JIN HUR[1], (Senior Member, IEEE)

[1]Electrical Engineering Department, Incheon National University, Songdo, Incheon 22012, South Korea
[2]Electrical Engineering Department, The University of Lahore, Lahore 54000, Pakistan

Corresponding author: Jin Hur (jinhur@inu.ac.kr)

This work was supported by Incheon National University under the Research Grant 2019-0420 and the Industrial Strategic Technology Development Program of Korea Evaluation Institute of Industrial Technology (KEIT) (No. 20006633).

ABSTRACT This paper proposes a special design of a dual stator radial type permanent magnet vernier machine (PMVM) having a yokeless rotor to improve the torque density. The PMVM model is designed with winding only in the outer stator, while the inner stator is kept auxiliary without winding. The proposed model reduced the overall volume of the machine, which in turn improved the torque density of the machine. The proposed configuration makes the design free from thermal and manufacturing issues due to the absence of inner stator winding. The detailed specifications and analysis results of the proposed model, such as torque, back EMF, inductance, and other features, are presented in this paper. The model is analyzed and compared with the dual stator radial type PMVM having a yokeless rotor and dual stator winding using the 2D-Finite Element Method (FEM) as well as 3D Co-simulation with Ansys Mechanical.

INDEX TERMS Dual stator PMVM, radial type, yokeless rotor, single stator winding, torque density, finite element method, co-simulation, thermal analysis.

I. INTRODUCTION

With increasing concerns over various developing applications such as electric vehicles and wind power generation, high-torque density machines, such as dual-rotor PM machines [1], harmonic machines [2], pseudo-PM machines [3], and transverse flux machines are gaining popularity in the industry as well as in academia. The direct-drive systems, which eliminate the use of mechanical gears, are very eagerly considered to be used in high-torque, low-speed applications such as electric vehicles, renewable energy conversion, elevators, and so on. However, the design of regular industrial machines for direct-drive performance may yield huge structures that suffer from poor operating characteristics. For example, the transverse flux PM machine having high torque density and pseudo PM machine with suitable operating characteristics were introduced [3]. But these machines have complex mechanical structures, and a very large amount of magnets were used in these machines, which made them unconventional structures for direct-drive operations.

Permanent magnet vernier machines (PMVMs) have been gaining much attraction for direct drive applications due to several features such as high torque density, low cogging torque, and excellent torque performance [4]–[7]. The operating principle of this machine is based on the magnetic flux modulation effect, which means that a small rotation of the rotor brings high flux change resulted in high torque production [8]. The design of the dual PM vernier machine and fractional pole vernier machine is also presented in [9], [10].

The PMVM was initially presented in [11], and its design details were discussed in [4]. The comparison of vernier machine and PM machine was presented in [12], and it was proved that the vernier machine could produce twice the back EMF as compared to the conventional PM machine. Therefore, the main characteristic of PMVM is the high torque density. Many topologies have been presented to improve the torque density of PMVMs. Generally, in PMVM, the rotor comprises a higher number of rotor permanent magnet poles than the stator poles in the machine. This results

The associate editor coordinating the review of this manuscript and approving it for publication was Paolo Giangrande.

TABLE 1. Comparison of different dual airgap PMVM topologies.

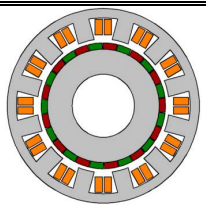 Model 1	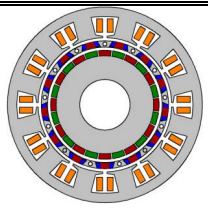 Model 2	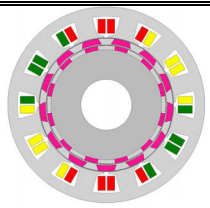 Model 3	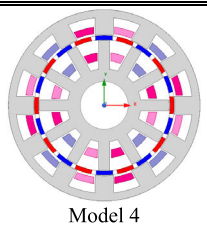 Model 4	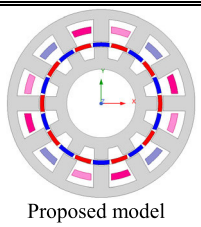 Proposed model
Minimum torque density as compared to the other models.	Torque density improved as compared to the reference model.	Torque density much improved as compared to the reference model.	Slightly reduced torque density as compared to the reference model.	Highest torque density as compared to the other models.
Magnet usage is higher as compared to other models.	Magnet usage is less than the reference model.	Magnet usage is less than the reference model.	Magnet usage is half than the reference model.	Magnet usage is similar to the reference model and minimum as compared to all other models.
Minimum core losses.	Core loss increased than the reference model.	Much higher core loss compared to the reference model.	Core loss slightly increased compared to the reference model.	Core losses are less than all the other dual airgap models.
Thermal and mechanical aspects are not considered.	Thermal and mechanical aspects are not considered.	Thermal and mechanical aspects are not considered.	Thermal and mechanical aspects are not considered.	Thermal and mechanical aspects are considered

TABLE 2. Specifications of DSRF-PMVM yokeless rotor models.

Parameter	Units	Values	
		DSW Model	SSW Model
Active Outer Diameter (D_o)	mm	120	
Active Inner Diameter (D_i)	mm	30	52
Outer Diameter of the inner stator	mm	81.1	72.7
Active Axial Length	mm	100	
Number of Rotor Pole Pairs	-	10	
Number of Stator Slots	-	12	
Number of Stator poles	-	4	
Length of Air Gap	mm	0.7	
Magnet Type	-	NdFeb35 (Br=1.23 T, Hc=-890 kA/m)	
Rotor Core Material	-	Non-magnetic SUS304	
Volume of Magnet	L	0.053	
Machine Volume	L	1.06	0.92
Number of conductors per Slot (outer/inner)	-	70/70	140
Slot Fill Factor (Outer/Inner Stator)	%	50/50	50
Rated Rotational Speed	rpm	400	
Phase Current	A_{rms}	4.7	

in an increased volume of PMVM, and the overall cost of manufacturing PMVM is also increased compared to other machines. A consequent pole PMVM was presented in [13] to decrease the flux leakage and improve the torque density of the machine. This machine produced almost 20% higher back EMF and 40% reduced magnet usage as compared to the conventional PMVM.

Furthermore, dual stator axial type PMVM with ring-type magnets was presented in [14] to improve the airgap flux density and reduce the flux leakage in the airgap while effectively utilizing the space within the machine structure. The dual stator PMVM was also presented in [15] and [16]. It was explained that the spoke type magnets with flux focusing capability could generate high torque density compared to the single airgap having the same dimensions. Another topology of dual stator PMVM was introduced in [17] to improve the torque density of the machine as compared to a single airgap PMVM. However, the cost of the machine was much increased due to the usage of PMs on the inner and outer stator. Compared to single stator PMVMs, the dual stator PMVM's structure is complex, and its mechanical support is also difficult. Moreover, since the induced EMF and flux linkage of inner and outer stator coils has some phase shift, the phase windings should be in series to avoid circulating currents, and these connections also introduce another distributed factor [18]. Furthermore, the dual stator PMVM with radial type structure always suffers from thermal issues due to the inner stator winding. In a dual airgap radial type structure, the inner stator is enclosed inside the rotor. The windings in the inner stator may produce heat during the operations that affect the temperature of the rotor magnets in the radial type structure. A topology of dual stator PMVM with single stator excitation was introduced in [19] to overcome the thermal and manufacturing issues of the inner stator winding. Additionally, the rotor iron yoke in dual stator structures caused the reduced flux linkage between inner and outer stator windings, which affects the machine's overall performance. This issue was addressed in [20] and was overcome by removing the iron core from the rotor. The machine resulted in a 50% volume reduction of PMs and 87% higher torque per machine volume than the similar volume of the machine having an iron yoke in the rotor.

This paper proposed a novel topology of dual stator PMVM with a yokeless rotor having a single stator winding to improve the torque density and overcome the thermal and manufacturing issues due to inner stator winding in the dual air gap model. The model combines the effects of a yokeless rotor and single stator winding to further increase the flux density of the machine. The proposed machine is compared with the reference dual stator PMVM having a yokeless rotor

TABLE 3. Performance comparison of DSRF-PMVM models wiith yokeless rotor.

Parameter	Units	Values	
		DSW Model	SSW Model
Back EMF (Inner/Outer)	V_{rms}	94.3	90.6
Phase Current	A_{rms}	4.7	
Torque Ripple	%	4.2	9.4
Average Torque	Nm	32.23	30.64
Machine Volume	L	1.06	0.92
Torque Density	Nm/L	30.4	33.4
Copper Loss	W	116.9	120.0
Core Loss	W	13.38	12.15
Total Loss	W	127.9	129.9
Efficiency	%	91.2	90.7

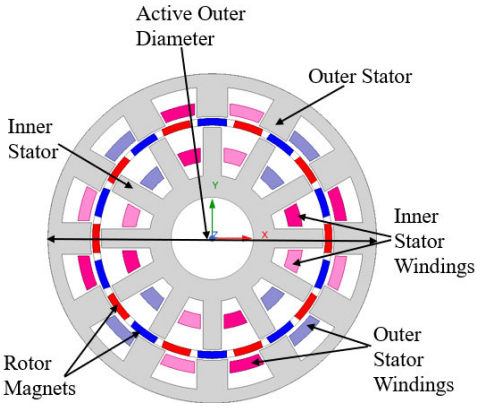

FIGURE 1. DSRF-PMVM DSW model with yokeless rotor.

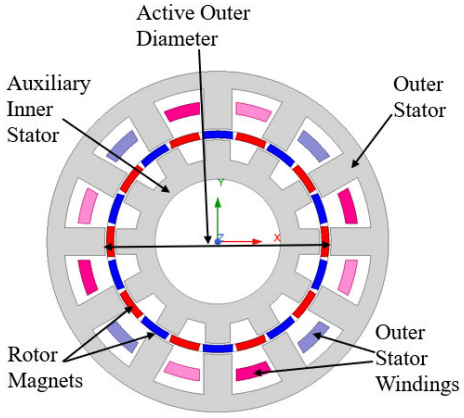

FIGURE 2. DSRF-PMVM SSW model with yokeless rotor.

and dual stator windings. The structure, working principle, and design concept of the dual stator PMVM model having a yokeless rotor and single stator winding (SSW) are presented. The machine is analyzed using the 2D finite element method (FEM) and the results are compared with the reference DSW model having the same outer diameter.

The proposed model is compared with the PMVM models presented in [18], [20], and [21] having similar dual airgap structures and similar outer dimensions. Table 1 shows the comparison of basic topologies and performance. Model 1 is a single airgap PMVM presented as a reference in [18], model 2 is the proposed model in [18], model 3 is the model proposed in [20], and model 4 is proposed in [21]. The detailed comparison based on the performance parameters values will be presented in section III.

II. PMVM MODEL TOPOLOGY, SPECIFICATIONS, AND WORKING PRINCIPLE

The topology of the reference dual stator radial flux (DSRF) PMVM having dual stator winding (DSW) configuration and a yokeless rotor is presented in Fig. 1. The reference machine consists of two stators and a sandwiched yokeless PM rotor. Both the stators are of conventional toothed pole structures to realize the flux modulation effect. The inner and outer stator has 12 slots and three-phase distributed type winding with 4 poles configuration. The rotor has 20 poles of NdFeb magnets and non-magnetic support to fix the magnets in place.

The layout of the proposed SSW machine is shown in Fig. 2. The outer stator and rotor have a similar structure as in the reference model. However, the dimensions of the outer stator and rotor are revised according to the design. The outer diameter of both the machines is kept constant.

The main difference between the two models is that the inner stator is kept auxiliary without winding in the SSW model. The windings from the inner stator are shifted to the outer stator, extending the outer stator inwards to accommodate the extra winding and managing the slot fill factor of 50% in the outer stator. The rotor diameter is also reduced to accommodate the extending outer stator. The inner stator slot size is reduced as it does not contain any windings and contributes to the flux modulation.

Consequently, the inner diameter of the inner stator is also increased, reducing the overall active volume of the machine. The volume of the reference machine is 1.06 Nm/L, whereas the volume of the proposed machine is 0.92 Nm/L. The magnet type and overall magnet volume are kept the same in both the reference and proposed model.

The working principle of the PMVMs is based on the interaction between the PM magnetic field and the rotating magnetic field by the stator windings, as mentioned in [12]. The relation between the number of stator slots, rotor poles, and stator poles follows the rule given in equation (1) as:

$$\pm P_s/2 = P_r/2 - S_s \tag{1}$$

where P_s, P_r, and S_s show stator winding poles, rotor poles, and stator slots, respectively.

The basic design of the reference model was obtained using the mathematical model in [18] and then the SSW model was redesigned following the design flow in Fig. 3. The design equations of the PMVM model based on the electromagnetic torque and power as mentioned in [18] are as under:

$$D_{g1}^2 L_{stk} = T_e/[(\sqrt{2}/20)\pi^2 k_w k_\delta \alpha_{p1} A B_{g1m}(Pr/Ps)cos\gamma] \tag{2}$$

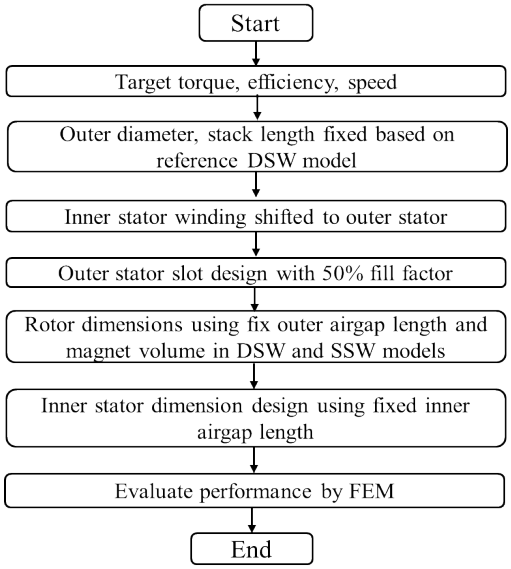

FIGURE 3. Design flow of the SSW model.

$$D_{g1}^2 L_{stk} = P_e/[(\sqrt{2}/20)\pi^3 k_w k_\delta \alpha_{p1} A B_{g1m}(f/Ps)cos\gamma] \quad (3)$$

where T_e and P_e represent the electromagnetic torque and power of the machine. k, k_w, k_δ, α_{p1}, A, B_{g1m}, P_r, P_s, f, D_{g1}, L_{stk} and cosγ show the winding factor, leakage factor, rotor pole arc, electrical loading, peak flux density in outer airgap, rotor pole pairs, stator pole pairs, the inner diameter of the outer stator, stack length and the power factor of the machine, respectively.

The detailed specifications of both models using (1) are presented in Table 2.

The operation of the PMVM is based on the flux modulation effect. The stator windings produce the low order harmonic field, and the rotor poles generate the high order harmonic field. The two fields produced by stator winding and rotor PMs interact to produce useful torque. This effect is called as "magnetic gearing effect," which results in a high torque production due to a high flux change by a small rotation of the rotor.

III. FINITE ELEMENT ANALYSIS AND COMPARISON OF EXISTING AND PROPOSED MODELS

In this section, the proposed DSRF-PMVM model having a yokeless rotor and SSW configuration is analyzed and compared with the reference model having a DSW configuration. Both the models are compared on similar no-load and load operating conditions at the speed of 400 RPM.

A. MESH SETTINGS AND FLUX PATH

The 2D transient FEM analysis was performed using surface-type mesh settings to the stators, rotor, and band in both models. The commercial software package of the Ansys Maxwell 20.0 version was used for this purpose. The maximum length of mesh was set to be 0.5 mm in load and no-load conditions.

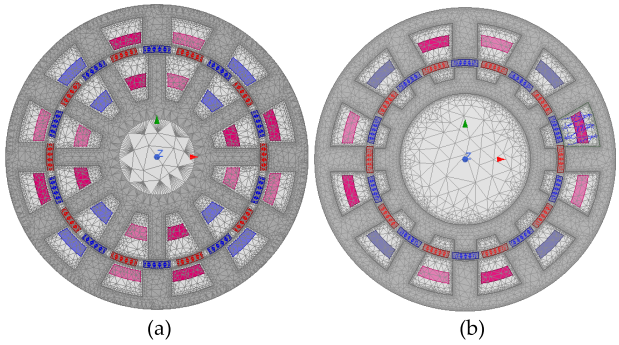

FIGURE 4. DSRF-PMVM mesh layout (a) DSW model (b) SSW model.

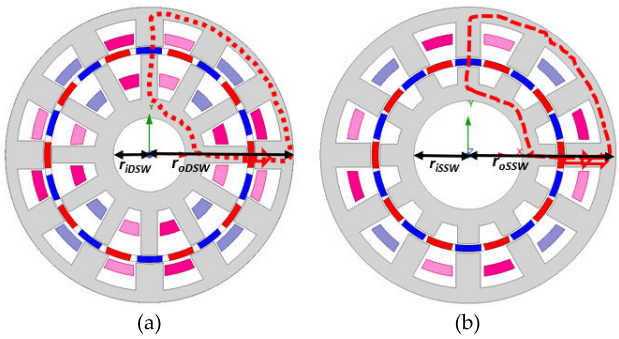

FIGURE 5. DSRF-PMVM flux path (a) DSW model (b) SSW model.

Fig. 4 shows the mesh layout in DSRF-PMVM having yokeless rotor with DSW and SSW topology.

B. RELUCTANCE AND INDUCTANCE

The reluctance of the machine plays an important role in the production of useful electromagnetic torque The reluctance of the machine depends upon the geometrical and material properties of the circuit. The reluctance of the machine is proportional to the mean length of the flux path. The flux paths of one pole of the reference model DSW and proposed model SSW are presented in Fig. 5(a) and Fig. 5(b), respectively. It is clear from Fig. 5(b) that the flux of the SSW model followed the shorter path due to the reduced size of the inner stator and increased active dia of the machine. The mean length of the flux path can be calculated as:

$$L_{mean} = 2^*\pi^*(r_o - r_i) \quad (4)$$

where L_{mean}, r_o, and r_i show the mean length of the flux path, active outer radius, and active inner radius of the machine. For DSW model:

$$L_{mean} = 2^*\pi^*(60 - 15) = 282.7 \text{ mm} \quad (5)$$

For SSW model:

$$L_{mean} = 2^*\pi^*(60 - 26) = 213.6 \text{ mm} \quad (6)$$

According to the above values, the flux path length in the SSW model is almost 25% reduced as compared to the DSW

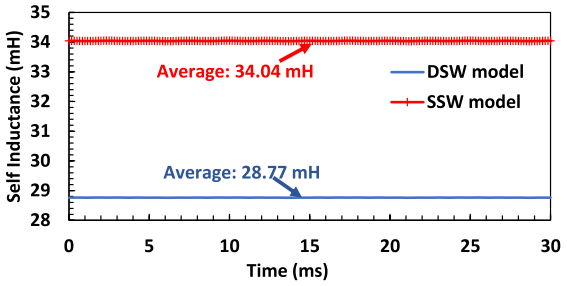

FIGURE 6. Self inductance comparison at load.

model. The shortening of the flux path, in turn, reduces the reluctance of the machine.

The inductance of the machine is directly proportional to the number of winding turns and inversely proportional to the reluctance of the machine as (7):

$$\mathrm{L} = \mathrm{N}^2/\mathscr{R}_{\mathrm{tot}} \tag{7}$$

where L, N, and $\mathscr{R}_{\mathrm{tot}}$ denote the inductance, the number of turns in the windings, and overall reluctance of the machine, respectively. As it is clear in (5) and (6), the reluctance of the DSRF-PMVM SSW model is reduced compared to the DSW model due to reduced mean flux path length. Hence, according to (7), the inductance should be increased in the SSW model. The self-inductance comparison of the DSW and SSWmodel is shown in Fig. 6. It can be seen that the mutual inductance of the SSW model is much higher as compared to the DSW model. The average value of mutual inductance of the DSW model is 28.77 mH as compared to the value of 34.04 mH in the SSW model. The mutual inductance of the proposed SSW model is 15.5% higher than the mutual inductance of the reference DSW model.

The reduction in the length of the flux path also helps to improve the torque density of the machine as mentioned in [22]. It will be discussed in the later section.

C. FLUX DENSITY, FLUX LINKAGE AND BACK EMF

Flux density in the machine is one of the important parameters to measure the torque capability of the machine. The flux density depends upon the number of poles in the machine as well as the inductance. The flux densities of the DSRF-PMVM model having a yokeless rotor with DSW and SSW topology at no-load and load cases are shown in Fig. 7 and Fig. 8. The no-load flux density of the DSW model is higher than the SSW model at the same scale due to the higher active volume of the DSW model. Whereas the flux density of the SSW model at load conditions is higher than the DSW model due to higher inductance in the SSW model.

The 3D comparison of flux densities in DSW and SSW models at load conditions is presented in Fig.9. It can be observed that the SSW model shows higher flux density at a similar scale as compared to the DSW model.

The comparison of flux linkages at no-load and load cases of the DSW and SSW model is presented in Fig. 10 and

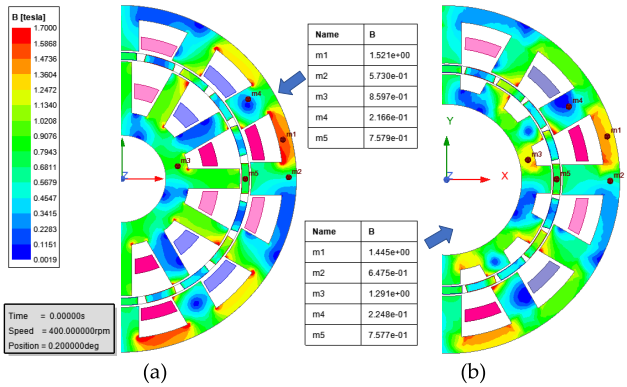

FIGURE 7. Flux densities in DSRF-PMVM at no-load (a) DSW model (b) SSW model.

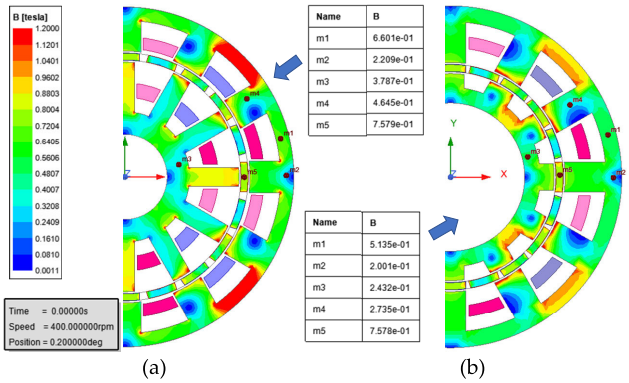

FIGURE 8. Flux densities in DSRF-PMVM at load (a) DSW model (b) SSW model.

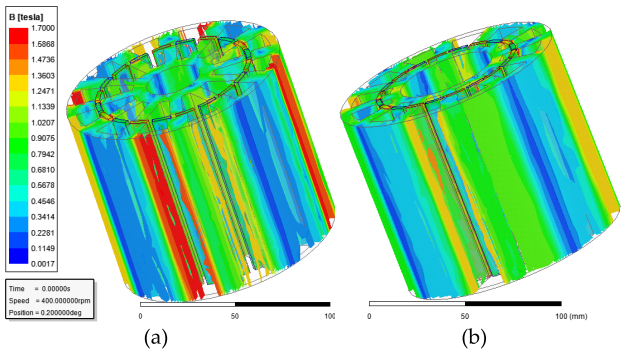

FIGURE 9. Flux densities in DSRF-PMVM at load in 3D (a) DSW model (b) SSW model.

Fig. 11. The no-load flux linkage of the DSW model is higher as compared to the SSW model. Whereas, the RMS value of flux linkage of the SSW model at load conditions is slightly higher than the DSW model due to the increased inductance at load conditions.

The back EMF comparison of the DSW and SSW models is shown in Fig. 12. The RMS value of back EMF at the rated speed of 400 rpm in the proposed SSW model is 90.6 V which is 4% reduced as compared to the 94.3 V back EMF of the reference model DSW due to the reduced size of the

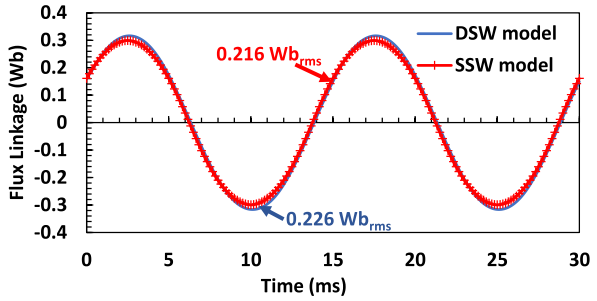

FIGURE 10. Flux Linkage in DSRF-PMVM at no-load.

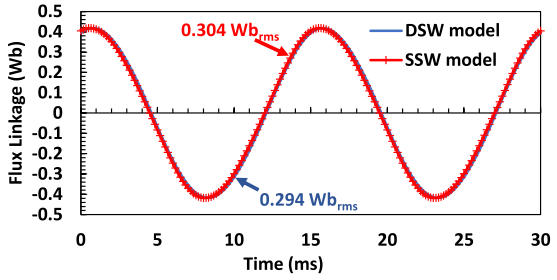

FIGURE 11. Flux Linkage in DSRF-PMVM at load.

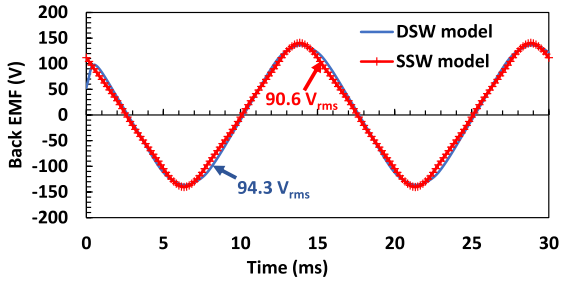

FIGURE 12. Back EMF comparison in DSRF-PMVM.

TABLE 4. Performance comparison at overload conditions.

Parameter	Units	Values	
		DSW Model	SSW Model
Phase Current	A_{rms}	7.05	
Torque Ripple	%	9.2	10.3
Average Torque	Nm	45.77	45.71
Machine Volume	L	1.06	0.92
Torque Density	Nm/L	43.17	49.8
Copper Loss	W	263.6	270.4
Core Loss	W	19.1	13.93
Total Loss	W	282.7	284.3
Efficiency	%	87.2	87.1

proposed model. This reduction is comparable to the benefits of improved torque density and other features associated with the proposed single winding model.

D. OUTPUT TORQUE, TORQUE DENSITY, AND RIPPLE

The torque waveforms of the reference DSW model and the proposed SSW model are compared in Fig. 13 at rated load conditions. The average torque of the proposed machine is 30.64 Nm, whereas the average value of torque for the

TABLE 5. Performance comparison of different topologies.

Parameter	Model 1	Model 2	Model 3	Model 4	Proposed Model
Rotor type	Yoke	Yoke	Yoke	Yokeless	Yokeless
Magnetization type	Halbach	Halbach	Halbach	Cartesian	Cartesian
Rated torque (Nm)	7.7	8.9	12.6	32.23	30.64
Machine Volume (L)	1.36	1.36	1.36	1.06	0.92
Torque density (Nm/L)	5.7	6.4	9.3	30.4	33.4
Magnet volume (L)	0.82	0.123	0.092	0.053	0.053
Core loss (W)	7.0	15	19.9	13.38	12.15
Thermal analysis	x	x	x	x	✓
Mechanical Analysis	x	x	x	x	✓
Efficiency	75.8	77.2%	81%	91.2	90.7

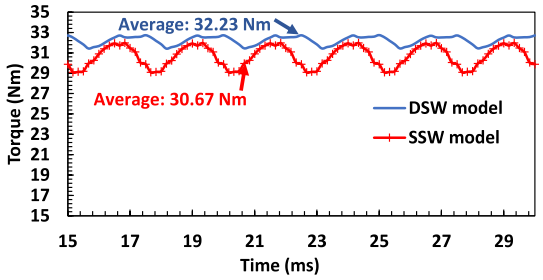

FIGURE 13. Torque comparison in DSRF-PMVM.

existing machine is 32.23 Nm. However, the machine volume of the proposed SSW model is 0.92 L, whereas the machine volume of the existing reference DSW model is 1.06 L. Hence, the torque density of the proposed SSW model is improved as compared to the DSW model. The torque density of the proposed model is 33.4 Nm/L as compared to the 30.4 Nm/L value of torque density of the existing DSW model. The comparison Table 3 also reveals that the torque density of the proposed SSW model is improved by 9% as compared to the existing DSW model.

The torque ripple of the existing reference DSW model is 4.2% whereas that of the proposed SSW model is 9.4%. This is a drawback of the proposed model which is due to the increased outer stator slot depth which in turn increases the overall permeance variation in the outer airgap. Moreover, the improvement in the torque density is significant along with the benefits of reduced thermal and manufacturing problems caused due to the inner stator winding as compared to the existing DSW model.

E. CORE LOSS AND EFFICIENCY

The efficiency of the two models is calculated using core losses in the stator cores P_{core} and copper losses P_{cu} in the windings of inner and outer stators. The core loss is obtained from the 2D-FEM simulation results and the results of DSW and SSW models are compared in Fig. 14. The core loss of the proposed model is less than the reference DSW model due to the reduced active volume of the SSW model. Both

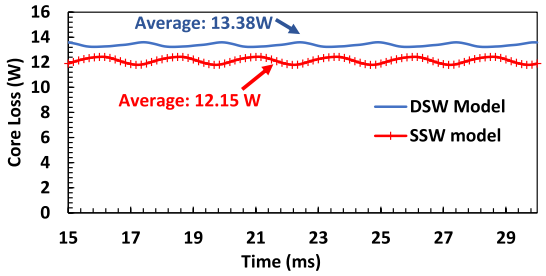

FIGURE 14. Core loss comparison in DSRF-PMVM.

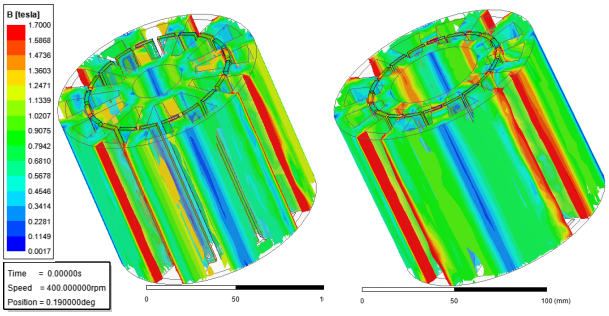

FIGURE 15. Flux densities in DSRF-PMVM at overload in 3D (a) DSW model (b) SSW model.

the machines have the same number of turns but the length of winding turns in the proposed SSW model was slightly increased while shifting the winding of the inner stator to the outer stator due to the higher radius of the outer stator.

The copper losses were calculated using the winding resistance as (6):

$$P_{cu} = 2 \times m \times I_{rms}^2 \times R_{ph} \tag{8}$$

where m represents the number of phases, I_{rms} show the RMS value of the input phase current, and R_{ph} is the phase resistance of the winding. The copper loss of the DSW model was calculated to be 116.9 W, whereas the value of copper loss for the proposed SSW model is 120.0 W as calculated using (6).

The efficiency of the models is calculated using the eq. (7) based on the core and copper losses as:

$$\eta = P_{out}/(P_{out} + P_{loss}) \times 100 \tag{9}$$

Based on the above formula, the efficiency of the reference DSRF-PMVM DSW model was found to be 91.2% and the value of efficiency for the proposed SSW model is calculated as 90.7%. The efficiency of the proposed SSW model is almost equal and comparable to the benefits of improving torque density and improved thermal and mechanical conditions as compared to the DSW model due to the absence of the inner stator winding. The power factor of the proposed SSW model is 0.71 as compared to the 0.8 power factor of the reference model. The power factor can be improved by certain optimization processes.

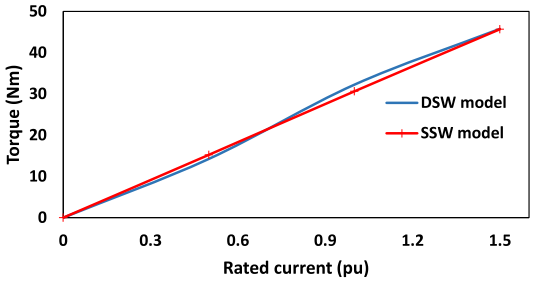

FIGURE 16. Torque profile at rated and overload current.

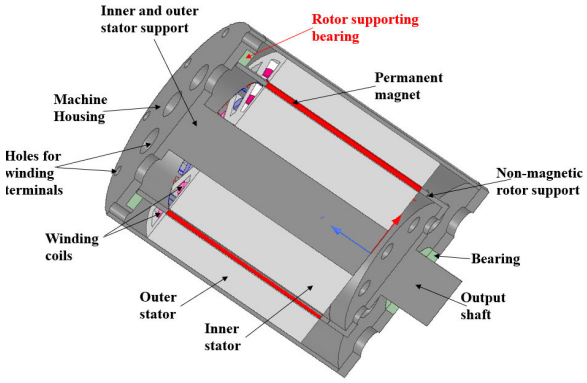

FIGURE 17. Cross-sectional view of DSRF-PMVM DSW model.

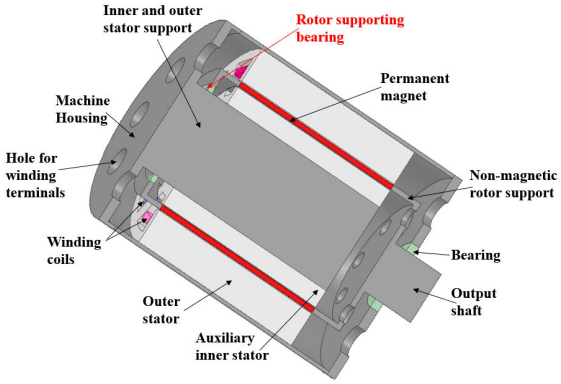

FIGURE 18. Cross-sectional view of DSRF-PMVM SSW model.

F. OVERLOAD CAPABILITY COMPARISON

The overload capacity of the reference DSW model and proposed SSW model is compared by operating at 1.5 times higher than the rated current. The 3D flux density at load conditions is compared in Fig. 15, and the detailed results are compared in Table 4. Fig. 15 shows that both the models show almost similar flux densities at a similar scale of reference at overload conditions. Fig. 16 shows the torque profile of the DSW and SSW models from zero to overload 1.5 p.u. current. Moreover, the comparison table of performance parameters also explains that at overload conditions, the performance gap of the DSW and SSW model is much reduced as compared to the performance at rated load condition. For example, the

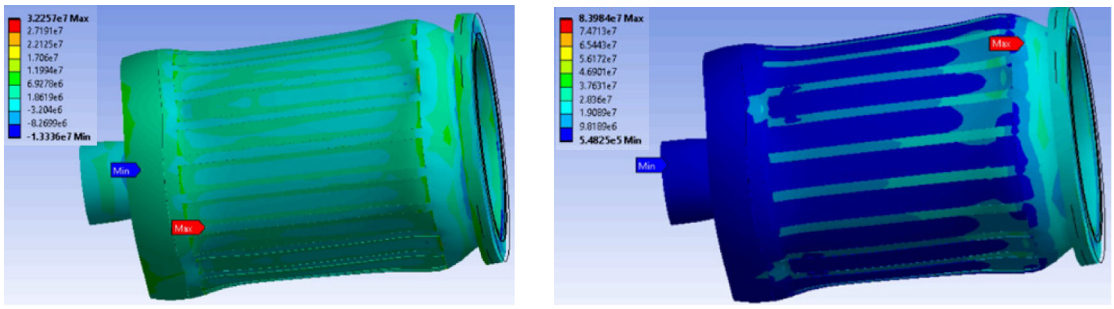

(a) (b)

FIGURE 19. Mechanical analysis of all rotating parts of DSRF-PMVM DSW model at load (a) Maximum principal stress (b) Equivalent stress.

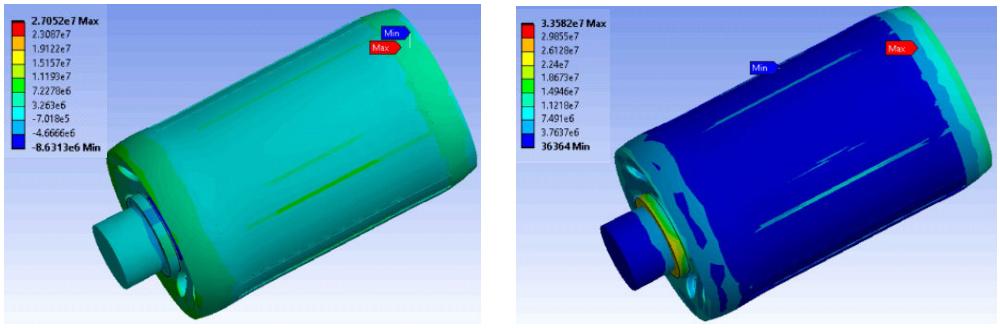

(a) (b)

FIGURE 20. Mechanical analysis of all rotating parts of DSRF-PMVM SSW model at load (a) Maximum principal stress (b) Equivalent stress.

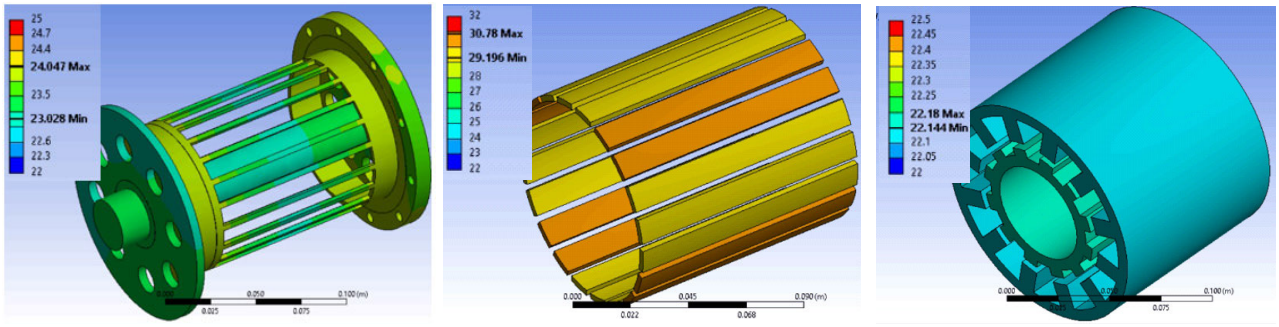

(a) (b) (c)

FIGURE 21. Thermal Analysis of DSRF-PMVM DSW model at no-load (a) Rotor and stator supports (b) Permanent magnets (c) Inner and outer stator.

torque ripple difference is reduced to only 1.1% as compared to the 5.2% difference at rated conditions. The average torque of the SSW model is almost similar to the DSW model at overload conditions, whereas the torque density of the SSW model is much increased. The efficiency of the SSW model is also similar to the DSW model at overload conditions. So overall we can conclude that the SSW model performs much better at overload conditions as compared to the reference DSW model.

The different PMVM models presented in Table 1 are compared based on the performance parameters. Table 5 presents the comparison of different dual airgap topologies based on their performance parameters. It can be seen from Table 5 that the torque density of the proposed model is the highest among all the other models. Moreover, the core loss of the proposed model is also lower as compared to other dual airgap models. The presented paper also considers the thermal and mechanical structure of the proposed SSW model which is not considered in other reference papers.

G. MECHANICAL ANALYSIS

The cross-sectional 3D views of the DSRF-PMVM model having reference DSW topology and proposed SSW topology are shown in Fig. 17 and Fig. 18, respectively.

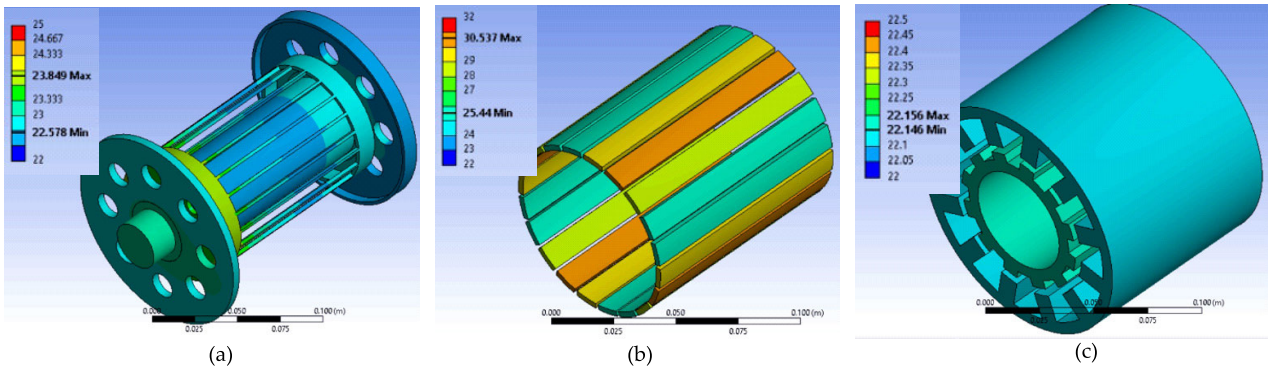

FIGURE 22. Thermal analysis of DSRF-PMVM SSW model at no-load (a) Rotor and stator supports (b) Permanent magnets (c) Inner and outer stator.

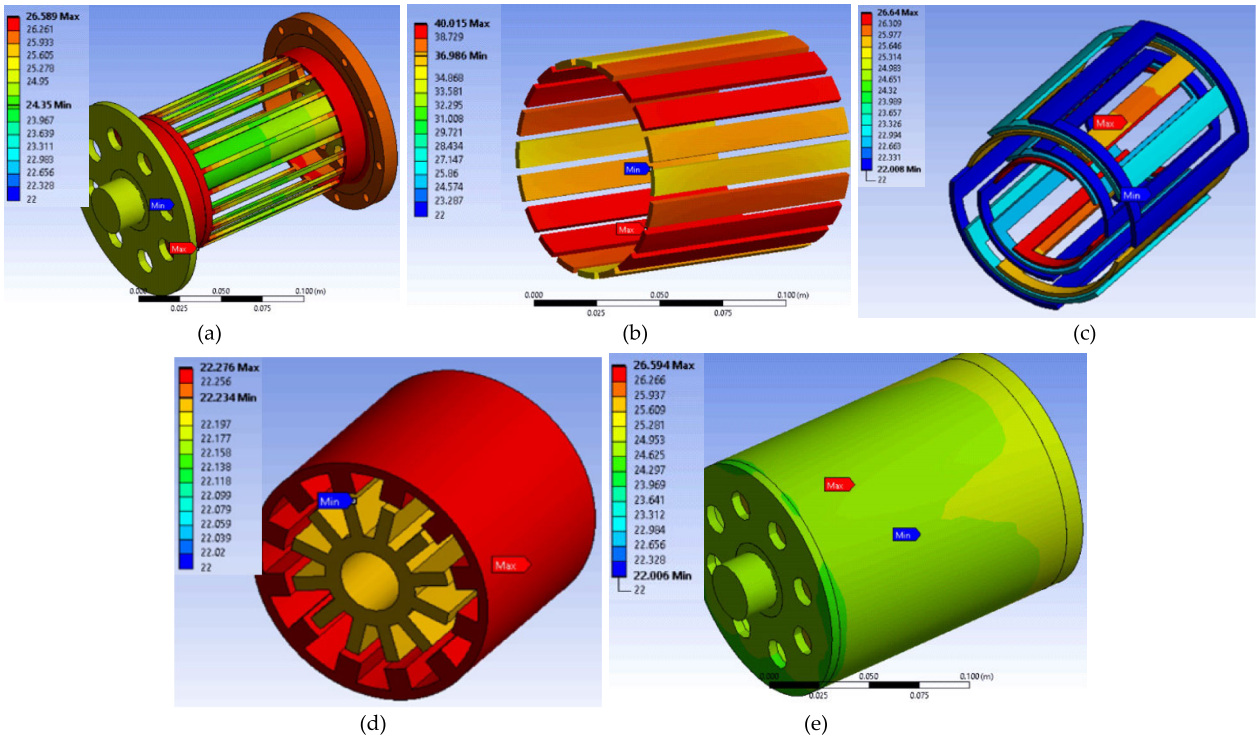

FIGURE 23. Thermal analysis of DSRF-PMVM DSW model at load (a) Rotor and stator supports (b) Rotor Magnets (c) Windings (d) Inner and outer stators (e) Complete machine.

According to Fig. 17, the rotor in the DSW model has a U-shape structure where one side (down) is connected to the output shaft for load connections, and the other side (up) is open to allow the inner stator winding terminals to connect to the outer stator. This type of rotor structure could have a possible risk of vibrations during the operation of the machine in load conditions. On the other hand, the SSW model shown in Fig. 18 contains a closed drum-shaped rotor that is connected to the central stator shaft via a support bearing. The inner stator is auxiliary, without winding, so the rotor can be closed and connected to the shaft similar to the conventional radial type structures. This closed drum-shaped structure allows the rotor to rotate without the risk of possible vibrations during load operations.

The stress analysis was performed on the rotating parts of the reference and proposed models to analyze the vibrations, using co-simulation between Ansys Maxwell and Ansys Mechanical. The results of structural analysis on the reference and proposed models are presented in Fig. 19 and Fig. 20.

Figure 19 (a) and Fig 20(a) show the maximum principal stress on the reference DSW model's rotor and the proposed SSW model's rotor, respectively. It can be seen that the maximum principal stress on the proposed SSW model's

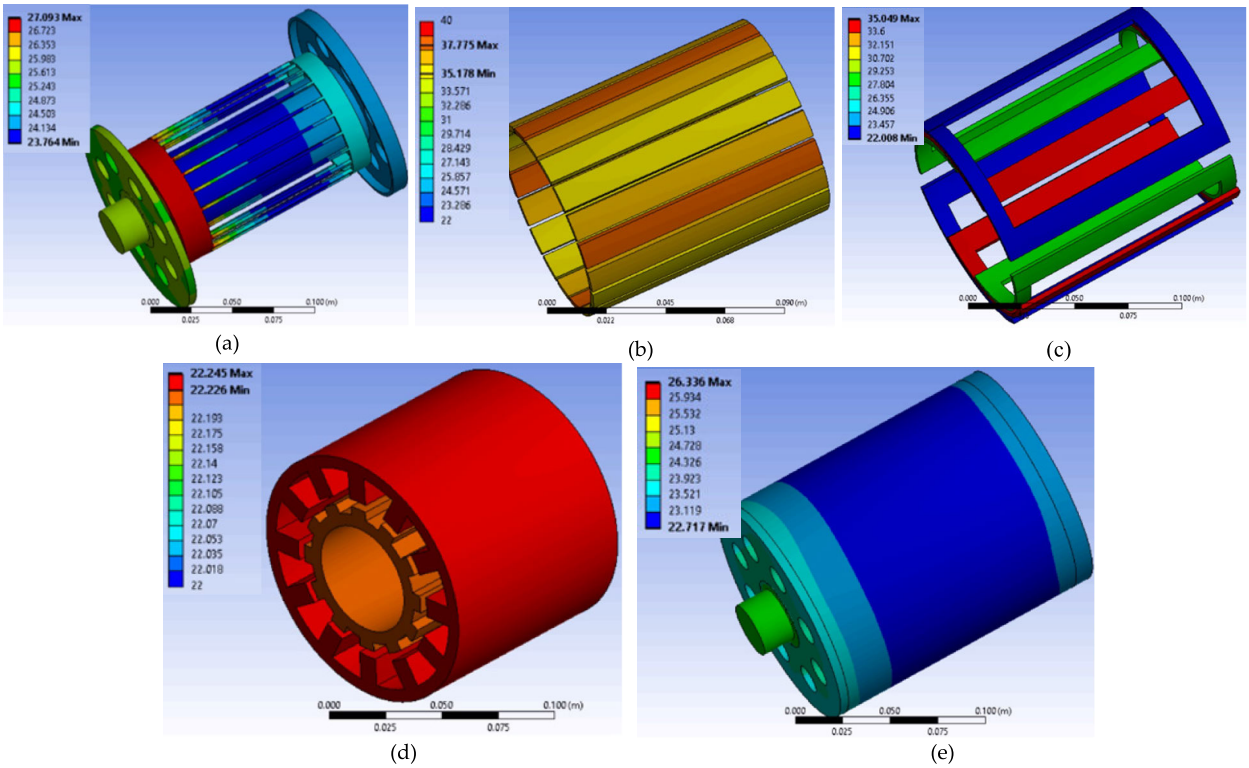

FIGURE 24. Thermal analysis of DSRF-PMVM SSW model at load (a) Rotor and stator supports (b) Rotor magnets (c) Windings (d) Inner and outer stators (e) Complete machine.

rotor (2.70 Pa) is much less as compared to the reference DSW model (3.23 Pa).

Moreover, the results of equivalent stress are shown in Fig. 19(b) and Fig. 20(b). The maximum value of the equivalent stress on the reference DSW model's rotor is 8.4*10^7 Pa, whereas the maximum equivalent stress on the SSW model's rotor is 3.4*10^7 Pa. The figures also show the higher stress in form of deformation in the DSW model's rotor. Therefore, it can be concluded that the SSW model performs better in terms of structural configuration as compared to the DSW model.

H. THERMAL ANALYSIS

This section presents the thermal analysis results performed on both the reference DSW model and proposed SSW models. The thermal analysis is performed using co-simulation between Ansys 3D and Ansys mechanical on similar conditions. The results are presented in Fig. 21, 22, 23, and 24.

Fig. 21 and Fig. 22 show the results of no-load analysis on DSW and SSW models, respectively. At similar conditions of no-load analysis, both the models show similar temperature rises due to the similar volume of magnets used in both models. Fig. 21(a) shows that at the same scale, most parts of the stator and rotor supports show higher temperature as compared to the temperature in counterparts in the SSW model, as shown in Fig. 22(a). Moreover, the temperature of the magnets also shows a slightly higher temperature in the DSW model as compared to SSW models, as shown in Fig. 21(b) and Fig. 22(b). As shown in Fig 21(c) and Fig. 22(c), the inner and outer stators show a similar temperature at no load.

The thermal analysis results of the reference DSW model and the proposed SSW model at load conditions are presented in Fig. 23 and Fig. 24, respectively. Comparing Fig. 23(a) and 24(a), it can be seen that the temperature of the rotor cage shows a slightly high temperature at the shaft side, whereas the temperature of the whole cage is higher in the case of the DSW model. As shown in Fig. 23 (b) and 24(b), the maximum temperature of the magnets is reduced to 37.7°C in the SSW model as compared to the value of 40.0 °C in the DSW model. The windings of the DSW model show a temperature of 26°C as compared to the winding temperature of 35°C in the SSW model, as presented in Fig. 23(c) and Fig. 24(c). The SSW model has double winding turns in the outer stator, while the same winding turns in the DSW model are divided into outer and inner stators. Double winding turns with the same amount of current show the higher temperature in the SSW model. But this temperature is still less than the minimum operating temperature of 40°C of the air-cooled machines.

Moreover, the inner and outer stator core show similar temperatures in both DSW and SSW models, as shown in Fig. 23(d) and Fig. 24(d). The whole machine temperature of the proposed SSW model has less value than the whole

machine temperature of the reference DSW model, as shown in Fig. 23(e) and 24 (e), respectively. Therefore, it can be concluded that the thermal performance of the proposed SSW model is better than the reference DSW model.

IV. CONCLUSION

A special topology of DSRF-PMVM is proposed in this paper to improve the torque density of the machine. The proposed SSW model contains a yokeless rotor and an auxiliary inner stator structure without winding. The proposed SSW model is compared with the reference DSW model, and the results reveal that the torque density of the proposed model is improved while reducing the core loss due to the reduction of overall machine volume. Moreover, the thermal and mechanical analysis of the reference and proposed models revealed that the proposed model performs better in terms of thermal and mechanical aspects of the machine as compared to the reference model having dual stator windings. The thermal analysis also proved that the proposed model is a better choice to remove the heat from the inner parts of the motor. However, the efficiency of the proposed SSW model is slightly reduced due to a slight increase in the copper losses while shifting the windings from the inner stator to the outer stator. This slight reduction in the efficiency can be considered the tradeoff for the benefits of improved thermal and mechanical conditions due to the absence of inner stator winding in the proposed SSW model.

REFERENCES

[1] R. Qu and T. A. Lipo, "Dual-rotor, radial-flux, toroidally wound, permanent-magnet machines," *IEEE Trans. Ind. Appl.*, vol. 39, no. 6, pp. 1665–1673, Nov./Dec. 2003.

[2] L. Jian, G. Xu, C. C. Mi, K. T. Chau, and C. C. Chan, "Analytical method for magnetic field calculation in a low-speed permanent-magnet harmonic machine," *IEEE Trans. Energy Convers.*, vol. 26, no. 3, pp. 862–870, Sep. 2011.

[3] K. Atallah, J. Rens, S. Mezani, and D. Howe, "A novel 'Pseudo' direct-drive brushless permanent magnet machine," *IEEE Trans. Magn.*, vol. 44, no. 11, pp. 4349–4352, Nov. 2008.

[4] A. Toba and T. A. Lipo, "Generic torque-maximizing design methodology of surface permanent-magnet Vernier machine," *IEEE Trans. Ind. Appl.*, vol. 36, no. 6, pp. 1539–1546, Nov./Dec. 2000.

[5] S. L. Ho, S. Niu, and W. N. Fu, "Design and comparison of Vernier permanent magnet machines," *IEEE Trans. Magn.*, vol. 47, no. 10, pp. 3280–3283, Oct. 2011.

[6] L. Wei and T. Nakamura, "A novel dual-stator hybrid excited permanent magnet Vernier machine with Halbach-array PMs," *IEEE Trans. Magn.*, vol. 57, no. 2, pp. 1–5, Feb. 2021, doi: 10.1109/TMAG.2020.3012193.

[7] D. Li, R. Qu, and T. A. Lipo, "High-power-factor Vernier permanent-magnet machines," *IEEE Trans. Ind. Appl.*, vol. 50, no. 6, pp. 3664–3674, Nov. 2014.

[8] T. Zou, D. Li, R. Qu, D. Jiang, and J. Li, "Advanced high torque density PM Vernier machine with multiple working harmonics," *IEEE Trans. Ind. Appl.*, vol. 53, no. 6, pp. 5295–5304, Nov./Dec. 2017.

[9] Q. Lin, S. Niu, F. Cai, W. Fu, and L. Shang, "Design and optimization of a novel dual-PM machine for electric vehicle applications," *IEEE Trans. Veh. Technol.*, vol. 69, no. 12, pp. 14391–14400, Dec. 2020, doi: 10.1109/TVT.2020.3034573.

[10] C. Shi, R. Qu, D. Li, X. Ren, Y. Gao, and Z. Chen, "Analysis of the fractional pole-pair linear PM Vernier machine for force ripple reduction," *IEEE Trans. Ind. Electron.*, vol. 68, no. 6, pp. 4748–4759, Jun. 2021, doi: 10.1109/TIE.2020.2991932.

[11] A. Ishizaki, "Theory and optimum design of PM Vernier motor," in *Proc. 7th Int. Conf. Electr. Mach. Drives*, Durham, U.K., Sep. 1995, pp. 208–212.

[12] Z. S. Du and T. A. Lipo, "Torque performance comparison between a ferrite magnet Vernier motor and an industrial interior permanent magnet machine," *IEEE Trans. Ind. Appl.*, vol. 53, no. 3, pp. 2088–2097, May/Jun. 2017.

[13] D. Li, R. Qu, J. Li, and W. Xu, "Consequent-pole toroidal-winding outer-rotor Vernier permanent-magnet machines," *IEEE Trans. Ind. Appl.*, vol. 51, no. 6, pp. 4470–4481, Nov./Dec. 2015.

[14] F. Zhao, M.-S. Kim, B.-I. Kwon, and J.-H. Baek, "A small axial-flux Vernier machine with ring-type magnets for the auto-focusing lens drive system," *IEEE Trans. Magn.*, vol. 52, no. 7, Jul. 2016, Art. no. 8204604, doi: 10.1109/TMAG.2016.2526040.

[15] B. Kim and T. A. Lipo, "Analysis of a PM Vernier motor with spoke structure," *IEEE Trans. Ind. Appl.*, vol. 52, no. 1, pp. 217–225, Jan./Feb. 2016.

[16] N. Baloch, S. Khaliq, and B.-I. Kwon, "HTS dual-stator spoke-type linear Vernier machine for leakage flux reduction," *IEEE Trans. Magn.*, vol. 53, no. 11, Nov. 2017, Art. no. 8111104.

[17] Y. Gao, R. Qu, D. Li, H. Fang, J. Li, and W. Kong, "A novel dual-stator Vernier permanent magnet machine," *IEEE Trans. Magn.*, vol. 53, no. 11, Nov. 2017, Art. no. 8111104.

[18] D. Li, R. Qu, W. Xu, J. Li, and T. A. Lipo, "Design procedure of dual-stator spoke-array Vernier permanent-magnet machines," *IEEE Trans. Ind. Appl.*, vol. 51, no. 4, pp. 2972–2983, Jul./Aug. 2015.

[19] M. R. Siddiqi, S. Khaliq, J.-W. Kwon, and B.-I. Kwon, "Optimal design of dual stator spoke type Vernier machine considering armature winding placement," *Int. J. Appl. Electromagn. Mech.*, vol. 59, no. 3, pp. 921–930, Mar. 2019.

[20] N. Baloch, B.-I. Kwon, and Y. Gao, "Low-cost high-torque-density dual-stator consequent-pole permanent magnet Vernier machine," *IEEE Trans. Magn.*, vol. 54, no. 11, Nov. 2018, Art. no. 8206105, doi: 10.1109/TMAG.2018.2849082.

[21] M. R. Siddiqi, T. Yazdan, J.-H. Im, M. Humza, and J. Hur, "Design and analysis of a dual airgap radial flux permanent magnet Vernier machine with yokeless rotor," *Energies*, vol. 14, no. 8, p. 2311, Apr. 2021.

[22] F. Chai, S. Cui, and S. Cheng, "Performance analysis of double-stator starter generator for the hybrid electric vehicle," *IEEE Trans. Magn.*, vol. 41, no. 1, pp. 484–487, Jan. 2005.

MUDASSIR RAZA SIDDIQI was born in 1991. He received the B.Sc. degree in electrical engineering from the University of Engineering and Technology, Taxila, Pakistan, in 2012, and the M.S. degree in electrical engineering from the Energy Conversion System Laboratory, Hanyang University, South Korea, in 2017. He is currently pursuing the Ph.D. degree with the Department of Electrical Engineering, Incheon National University, South Korea.

From 2017 to 2018, he was a Researcher at Nex-M Protohouse, Ansan, South Korea. His research interest includes the design and control of electric machines.

TANVEER YAZDAN was born in Punjab, Pakistan. He received the bachelor's degree in electrical engineering from the University of Engineering and Technology, Taxila, Pakistan, in 2010, and the M.S. and Ph.D. degrees in electrical engineering from Hanyang University, South Korea, in 2018.

From 2010 to 2013, he worked as an Assistant Manager with Karachi-Electric Company, Pakistan. He is currently working as an Assistant Professor with The University of Lahore, Pakistan. His research interest includes the design and control of electric machines.

JUN-HYUK IM (Student Member, IEEE) was born in Daejeon, South Korea, in 1992. He received the B.S. and M.S. degrees in electrical engineering from Incheon National University, Incheon, South Korea, in 2017 and 2019, respectively, where he is currently pursuing the Ph.D. degree in electrical engineering.

His research interests include motor design, motor control, and fault diagnosis of motors.

YEOL-KYEONG LEE received the B.S. degree in electrical engineering from Incheon National University, Incheon, South Korea, in 2020, where he is currently pursuing the M.S. degree.

His research interests include motor design, motor control, and fault diagnosis of motors.

JIN HUR (Senior Member, IEEE) received the Ph.D. degree in electrical engineering from Hanyang University, Seoul, South Korea, in 1999.

From 1999 to 2000, he was a Postdoctoral Research Associate with the Department of Electric Engineering, Texas A&M University, College Station, TX, USA. From 2000 to 2001, he was a Research Professor of electrical engineering for BK21 projects at Hanyang University. From 2002 to 2007, he was the Director of the Intelligent Mechatronics Research Center, Korea Electronics Technology Institute (KETI), Puchon, South Korea, where he worked on the development of special electric machines and systems. From 2008 to August 2015, he was an Associate Professor with the School of Electric Engineering, University of Ulsan, Ulsan, South Korea. Since August 2015, he has been a Professor with the Department of Electrical Engineering, Incheon National University, Incheon, South Korea. He has authored and coauthored over 140 publications on electric machine design, analysis and control, and power electronics. He has one pending U.S. patent and 20 pending Korean patents. His current research interests include high-performance electrical machines, modeling, drives, new concept actuators for special purposes, and numerical analysis of electromagnetic fields.

Dr. Hur is an Associate Editor for IEEE TRANSACTION ON POWER ELECTRONICS.